Journal of Molecular Catalysis A: Chemical 411 (2016) 214–221

Contents lists available at ScienceDirect

Journal of Molecular Catalysis A: Chemical

journal homepage: www.elsevier.com/locate/molcata

Fabrication of hybrid mesoporous TiO_2–SiO_2(Et) supported Ni nanoparticles: An efficient and air/water stable catalyst

Wei Li[a,b,1], Haiyang Cheng[a,b,*], Weiwei Lin[a,b], Guanfeng Liang[a,b], Chao Zhang[a,b], Fengyu Zhao[a,b,*]

[a] State Key Laboratory of Electroanalytical Chemistry, Changchun Institute of Applied Chemistry, Chinese Academy of Sciences, Changchun 130022, PR China
[b] Laboratory of Green Chemistry and Process, Changchun Institute of Applied Chemistry, Chinese Academy of Sciences, Changchun 130022, PR China

ARTICLE INFO

Article history:
Received 12 September 2015
Received in revised form 14 October 2015
Accepted 26 October 2015
Available online 30 October 2015

Keywords:
Ni-based catalyst
Stability
Mesoporous TiO_2–SiO_2
Hydrophobicity

ABSTRACT

We prepared a series of mesostructured Ni/TiO_2–SiO_2(Et) hybrid catalysts with highly dispersed Ni nanoparticles and incorporated ethane-bridged organosilica moieties. Ni/TiO_2–SiO_2(Et) showed high activity in the hydrogenation of nitrobenzene in water, and it could be recycled for several times with a constant activity and selectivity. It was confirmed that Ni/TiO_2–SiO_2(Et) catalyst is of hydrophobicity as the ethane-bridged organosilica fragments were incorporated into the mesoporous framework, and so the Ni active species was protected without contacting with water to form the inactive Ni species. In particularly, the Ni/TiO_2–SiO_2(Et) catalyst was air-stable, it could remain good activity after being exposed to air for a week. Accordingly, this work developed a kind of hydrophobic Ni catalyst with high stability to water and air, which is expected to have a wide application in the hydrogenation reactions.

1. Introduction

More recently, the research on the nonprecious catalysts has attracted many interests, and the Ni-based catalysts have been paid more attention due to its low cost and moderate activity with comparing to the precious catalysts. However, the Ni catalysts are still far from the ideal application as they bear some intrinsic disadvantages [1–10]. For example, Raney Ni bears the severe corrosion and the pollution originating from catalyst preparation as well as the safety problem in storage and application [11,12]. To date, the supported Ni catalyst like Ni/TiO_2 was reported to be a promising candidate for nitro-compounds hydrogenation because of its high activity, easy availability, low price and safe in handling. TiO_2 as a reducible metal oxide support could be reduced at a high temperature to form suboxide TiO_x species ($x < 2$), and migrate to the surface of metal particles [13–16]. And so, the adsorbed N=O bond was polarized and highly susceptible to the hydrogen attack, resulting in a high turnover frequency (TOF) in the hydrogenation of nitro-compounds [15,16]. The similar results was also found in the hydrogenation of *o*-chloronitrobenzene (*o*-CNB) to *o*-chloroaniline (*o*-CAN), in which Ni/TiO_2 was much more active than Ni/ZrO_2, Ni/SiO_2 and Ni/γ-Al_2O_3 catalysts due to the interaction between Ni and TiO_x ($x < 2$) species [17].

More recently, water as a solvent or co-solvent has been well investigated for the catalytic hydrogenation reactions. The addition of appropriate amounts of water into methanol or ethanol, the reaction rate was enhanced dramatically for the selective hydrogenation of CNB over a series of metal supported catalysts [18–21], for example, when the molar ratio of water to methanol increased from 0 to 1, the reaction rates of the transfer hydrogenation of styrene and nitrobenzene (NB) over Pd-based catalyst were increased more than 3 times [18]. Furthermore, it was also reported that the increase in water content could raise the reaction rate of the hydrogenation of *p*-nitrophenol in both ethanol and dioxane solvents, and the highest reaction rate was obtained in pure water [22]. Moreover, it was found that minor amount of water (0.14–1 mL) could significantly promote hydrogenation of 6-chloro-2-nitrotoluene over Pd/C catalyst [23]. In our previous work, we found water could accelerate the reaction rate and improve the product selectivity largely in the hydrogenation of *o*-CNB and NB [24–25], because the interaction between water and *N*-phenyl-hydroxylamine (PHA) *via* OH—O and OH—N hydrogen bonding which accelerates the rate-determining step of PHA to aniline (AN), as the ν(N—O) of PHA presented a red-shift in the presence of water [25], besides, interfacial hydrogen bonding, OH—ONO between H_2O and NB molecules may weaken the N—O bond of NB [26], improve the hydrogenation of NB to PHA. Ni/TiO_2 was an effective catalyst for the hydrogenation of nitro-compounds, however, it

* Corresponding authors at: State Key Laboratory of Electroanalytical Chemistry, Changchun Institute of Applied Chemistry, Chinese Academy of Sciences, Changchun 130022, PR China. Fax: +86 431 8526 2410.
E-mail addresses: zhaofy@ciac.ac.cn, hycyl@ciac.ac.cn (F. Zhao).
[1] W. Li is currently with Triangle Tyre Co., Ltd., Weihai 264200, PR China.

http://dx.doi.org/10.1016/j.molcata.2015.10.023
1381-1169/

significantly deactivated in water, while its stability was improved significantly when coated with a layer of hydrophobic carbon, but the stronger adsorption of organic products on the carbon layer lowered the activity gradually during the recycles [27]. Therefore, it is of great interest and a big challenge to design a stable Ni catalyst for the aqueous phase hydrogenation.

Herein, a hybrid mesoporous TiO_2–SiO_2(Et) supported Ni nanoparticles (Ni/TiO_2–SiO_2(Et)) was prepared in $scCO_2$-expanded ethanol by using co-condensation, hydrothermal treatment technique. Ethane-bridged organosilica fragment ($O_{1.5}$–Si–CH_2CH_2–Si–$O_{1.5}$) was used as bridging component, which can improve the porosity and simultaneously increase the surface hydrophobic of catalyst. The structural and textural properties as well as the morphology of the Ni/TiO_2–SiO_2(Et) catalysts were well characterized and their catalytic performances (activity and stability) were evaluated and discussed with the hydrogenation of nitrobenzene in water.

2. Experimental

2.1. Chemical and reagents

Pluronic P123 (MW = 5800), and 1,2-bis-(triethoxysilyl) ethane (BTESE, 97%) were purchased from Sigma–Aldrich and used without further purification. Tetrabutyl titanate (TBT, 98 %) and $Ni(NO_3)_2{\cdot}6H_2O$ were obtained from Sinopharm Chemical Reagent Co. Ltd., Beijing, China. All other chemicals were analytical reagents and obtained from Beihua Fine Chemical Co., Beijing, China.

2.2. Preparation of mesoporous TiO_2–SiO_2(Et-x)

A series of the TiO_2–SiO_2(Et-x) materials were synthesized by the following process. Pluronic P123 (0.55 g) was dissolved with H_2O (16.9 mL) to obtain a clear solution, and then HCl (37.0%, 1.18 mL) was added. Subsequently, BTESE and TBT was added drop wise to the above solution at hourly intervals, successively. The resulting mixture was stirred at 40 °C for 24 h, and then heated up to 100 °C with a heating rate of 2 °C min^{-1} and hydrothermal treated for another 24 h. The molar ratio of P123/Ti/Si//HCl/H_2O in the starting material is 0.06/1.00/(0.20–1.00)/8.90/691. The resulting white solid product was filtered, washed with deionized water and ethanol, and then air-dried at 100 °C overnight. The final product was denoted as TiO_2–SiO_2(Et-x), where x represents the molar ratio of Si to Ti in the sample; herein, x = 0.2, 0.4, 0.6.

The preparation of $TiO_2{}^{meso}$ was similar to the TiO_2–SiO_2(Et-x) hybrid material as described above, except for without BTESE involved.

2.3. Preparation of Ni/TiO_2_SiO_2(Et-x)

The as-prepared TiO_2/SiO_2(Et-x) materials (100 mg) were well dispersed in ethanol solution (10 mL) of $Ni(NO_3)_2$ $6H_2O$ in a glass bottle under ultrasonic treatment. The dense colloidal solution was then transferred into an autoclave (50 mL), which subsequently was placed into an oil bath at 150 °C and then pumped CO_2 to form a homogeneous expanded fluid under rapid stirring (12.0 MPa). And then the reactor was heated to the reaction temperature of 200 °C, at which the pressure went up to *ca.* 22.0 MPa. After the reaction was performed for 2 h, the autoclave was cooled down to room temperature, and then CO_2 was released slowly. After centrifugation, the composites were collected and dried. The samples were reduced under H_2 flow at 350 °C for 2 h as confirmed by TPR (Fig. S1), the samples were collected and labelled as Ni/TiO_2–SiO_2(Et-x). Ni/$TiO_2{}^{meso}$ was prepared with similar procedure described above. Ni loading in the catalyst was about 17 wt% as determined by inductively coupled plasma atomic emission spectrometer (ICP-AES). Ni/TiO_2 was prepared according to our previous work [27].

2.4. Characterization of catalyst

Powder X-ray diffraction (XRD) was performed using a Bruker D8 Advance X-ray diffract meter with a Cu Kα source at 40 kV and 40 mA. The scans were performed from 0.6° to 5° at a 0.05°/min speed for low angle XRD (LXRD) and 10° to 90° at a 4°/min speed for wide angel XRD (WXRD).

Nitrogen porosimetry measurement was performed on a Micromeritics ASAP 2020 M instrument. The surface areas were calculated using the BET equation. Pore size distributions were calculated using the BJH model based on nitrogen desorption isotherms. The samples were treated under vacuum at 90 °C for 1 h and then 200 °C for 12 h.

Transmission electron microscopy (TEM) study was carried out with a JEOL JEM-2010 instrument at an accelerating voltage of 200 kV. The TEM samples were prepared by dispersing the catalyst powder in ethanol under ultrasonic for 5–10 min and then the resulted solution was dropped on a carbon film of copper grid.

^{13}C CP-MAS NMR spectrum was recorded on a Bruker AVANCE III 400WB spectrometer equipped with a 4 mm standard bore CP MAS. Chemical shift for ^{13}C CP-MAS NMR spectrum was referenced to the signal of adamantane ($C_{10}H_{16}$) standard (δCH_2 = 38.5 ppm).

X-ray photoelectron spectroscopy (XPS, VG Microtech 3000 Multilab) was used to examine the electronic properties of Ni on the surface of catalysts. The C 1 s peak at 284.6 eV arising from adventitious carbon was used as reference. This reference gives binding energy values with a precision of ±0.02 eV. The surface composition of the samples was determined from the peak areas of the corresponding lines using a Shirley type background and empirical cross section factors of XPS. Generally, the sample for XPS measurement is the fresh reduced Ni catalysts stored in ethanol with N_2 protection. For etching the surface layers, bombardment by argon ions with energy of 5000 eV was used.

2.5. Catalytic performance tests

Prior to reaction, the diffusion effect was checked by changing the size of catalyst and the stirring speed. The calcined catalysts were ground and separated by screen with a size from 140 (≤109 μm) and 180 meshes (≤80 μm). The results show that the reaction rate kept at a constant value with a particle size smaller than 140 meshes, indicating that the inner transfer resistance was removed. In addition, it is confirmed when the stirring speed was up to 800 rpm, the reaction rate did not increase further, indicating the external diffusion has been removed. As a result, the catalysts with a particle size smaller than 180 meshes (<80 μm) was used, and 1200 rpm was selected for the reactions to evaluate the catalytic performances.

Before reaction, the catalyst (40 mg) was freshly reduced in a quartz tube at appropriate temperature with H_2 flow 30 mL/min for 2 h; then, H_2 was changed to N_2 and the quartz tube was cooled down to room temperature. The reduced catalyst was transferred into a 50-mL stainless steel autoclave reactor in N_2 flow in which 3 mL nitrobenzene and 3 mL H_2O was added. The reactor was then sealed, and flushed with H_2 more than three times to remove the air and placed into a water bath preset to the reaction temperature for 15 min. Then, H_2 (5.0 MPa) was introduced into the reactor, and the reaction was started at 80 °C with an agitation speed of 1200 rpm. When the reaction was finished, the reactor was cooled to room temperature in ice-water bath and then vented hydrogen to ambient pressure. The liquid product was extracted with 10 mL diethyl ether and analyzed with a gas chromatograph (Shimadzu GC-2010, Rtx-5 capillary column) using a flame ionization

detector. Through GC–MS analysis, aniline (AN) was the main products besides several intermediates such as nitrosobenzene (NSB), *N*-phenylhydroxylamine (PHA), azoxybenzene (AOB), azobenzene (AB) and hydrazobenzene (HAB).

The catalytic performance of the catalysts was characterized quantitatively by the conversion of nitrobenzene and the selectivity of aniline which was calculated as follows:

$$\text{Conversion} = \frac{([\text{NB}]_0 - [\text{NB}]_t)}{[\text{NB}]_0} \times 100\%$$

$$\text{Selectivity} = \frac{\text{M}_{\text{AN}}}{(\text{M}_{\text{AN}} + \text{M}_{\text{by-products}})} \times 100\%$$

where $[\text{NB}]_0$ and $[\text{NB}]_t$ refers to the concentration of nitrobenzene at 0 and t h, respectively; M_{AN} and $\text{M}_{\text{by-products}}$ represents the amount of aniline and by-products (*e.g.*NSB, PHA and a series of azo-compounds identified by GC–MS), respectively. The GC results were collected with an internal standard method, and *o*-xylene was used as internal standard. The carbon balance was near 100% on the basis of the detected compounds of NB, NSB, PHA, AOB, AB and HAB.

For the catalyst recycling test, the reactions were operated with the same procedure as described above. After the first run finished, the catalyst was separated and used for the next run directly. In the recycles, the H_2 consumption was recorded by the pressure change at the interval time, the end of reaction was judged by the cease of pressure dropping.

3. Results

3.1. Preparation of mesostructured Ni/TiO$_2$–SiO$_2$(Et) catalyst

TiO_2–SiO_2(Et) hybrid materials were prepared by co-hydrolysis and condensation of TBT with bissilylated organic precursor (BTESE) in the presence of triblock copolymer surfactant P123, which was used as the structure directing reagent. Generally, the hydrolysis rate of BTESE was obviously slower than that of TBT. In order to successfully introduce $O_{1.5}$–Si–CH_2CH_2–Si–$O_{1.5}$ as bridging component into TiO_2 framework through —Ti—O—Si—C—C—Si—O— linkages, prehydrolysis of BTESE was proceeded at 40 °C for 1 h at the beginning of preparation [28,29]. Therefore, the mesostructured TiO_2-SiO_2(Et) hybrid materials were obtained with ethane-bridged organosilica moieties incorporating into the TiO_2 framework as confirmed by ^{13}C CP/MAS NMR spectrum in Fig. 1. The strong signal at δ of 5.57 ppm was attributed to carbon atoms of the ethane-bridged organosilica species, whereas the other three weak signals at δ = 17.06, 71.05, and 76.05 ppm were originated from carbon species in the residual surfactant P123 [30]. It also indicated that the ethane-moieties still existed in the samples after reduced at 350 °C, which was also determined by the results of TGA (Fig. S2). The weight loss increased with molar ratio increasing of Si to Ti (BTESE to TBT) at the temperature range of 30–800 °C, as the decomposition of the ethane-moieties in the matrix.

Meanwhile, the Ni nanoparticles were dispersed onto TiO_2–SiO_2(Et) using *sc*CO2-expanded ethanol technique as described in previous work [31,32]. Consequently, a series of mesostructured Ni/TiO_2–SiO_2(Et-x) catalysts were fabricated with a Ni loading controlled and a highly dispersed Ni nanoparticles on the surface and/or inside of pores. The structure and physical properties were characterized and examined by LXRD, TEM, and nitrogen porosimetry measurement. LXRD patterns of Ni/TiO_2–SiO_2(Et-x) samples (x = Si/Ti molar ratio, 0.2–0.6) exhibited a sole Bragg reflection at 2θ = 1.17° (Fig. 2), indicating that these materials have the uniformed mesopores. The nitrogen adsorption–desorption isotherms and pore size distribution of the as-prepared Ni-based catalysts are shown in Fig. 3. All

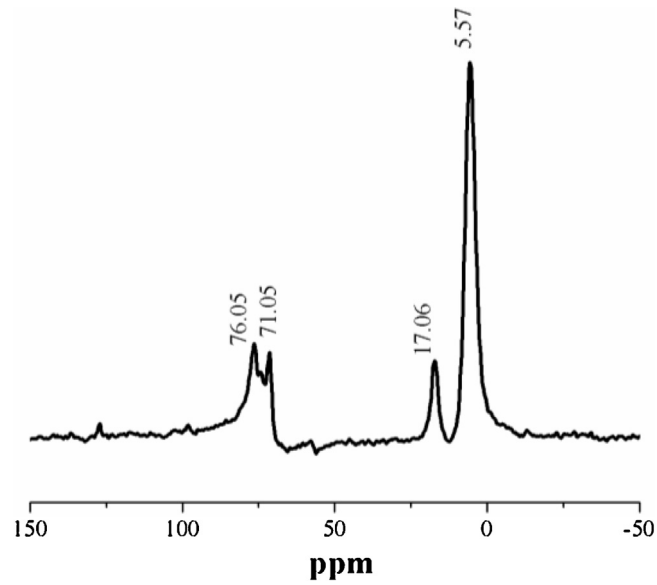

Fig. 1. ^{13}C CP/MAS NMR spectrum of Ni/TiO_2–SiO_2(Et-0.6).

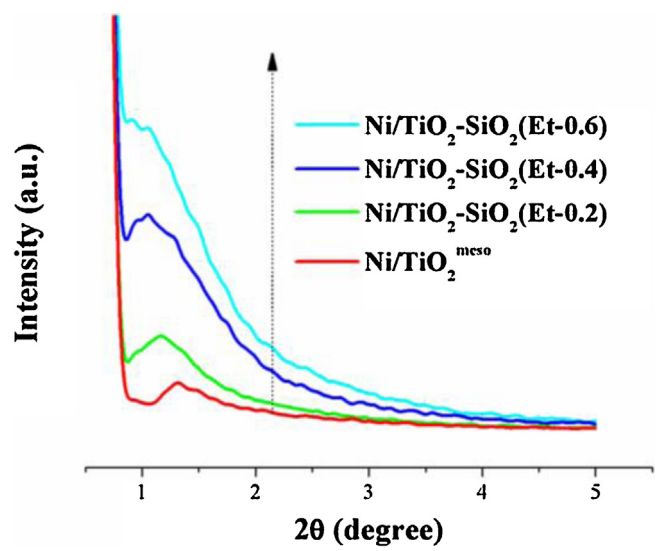

Fig. 2. LXRD patterns of Ni/TiO_2^{meso} and Ni/TiO_2–SiO_2(Et-x).

the tested samples, except Ni/TiO_2, displayed type IV isotherm, indicating the obtained Ni/TiO_2–SiO_2(Et-0.6) is of mesoporosity. Ni/TiO_2–SiO_2(Et-0.6) and Ni/TiO_2^{meso} exhibited H2 hysteresis loops with narrow BJH pore size distribution curves, suggesting that these catalysts possessed uniform pore with interconnecting channels. Additionally, the shape of hysteresis loop and the amount of volume absorbed of TiO_2–SiO_2(Et-0.6) are similar to the values of Ni/TiO_2–SiO_2(Et-0.6), implying that the dispersing process of Ni particles in scCO_2-expanded ethanol did not change the mesoporosity of TiO_2–SiO_2(Et-0.6). The similar results were also observed for Ni/$TiO_2^{meso}$and TiO_2^{meso} . However, Ni/TiO_2 showed H3 hysteresis loop with broad pore-size distribution. The textural parameters of the prepared catalysts and supports are summarized in Table 1, the BET surface area, the pore diameter, and the pore volume of Ni/TiO_2–SiO_2(Et-0.6) was 404 m^2/g, 6.3 nm and 0.54 cm^3/g, but these values of Ni/TiO_2^{meso} was 203 m^2/g, 3.8 nm and 0.23 cm^3/g, respectively. Compared with the support TiO_2–SiO_2(Et-0.6), the BET surface area and the pore volume of the supported Ni catalyst of Ni/TiO_2–SiO_2(Et-0.6) presented a slightly decrease. Moreover, the porosity of Ni/TiO_2^{meso} prepared using the

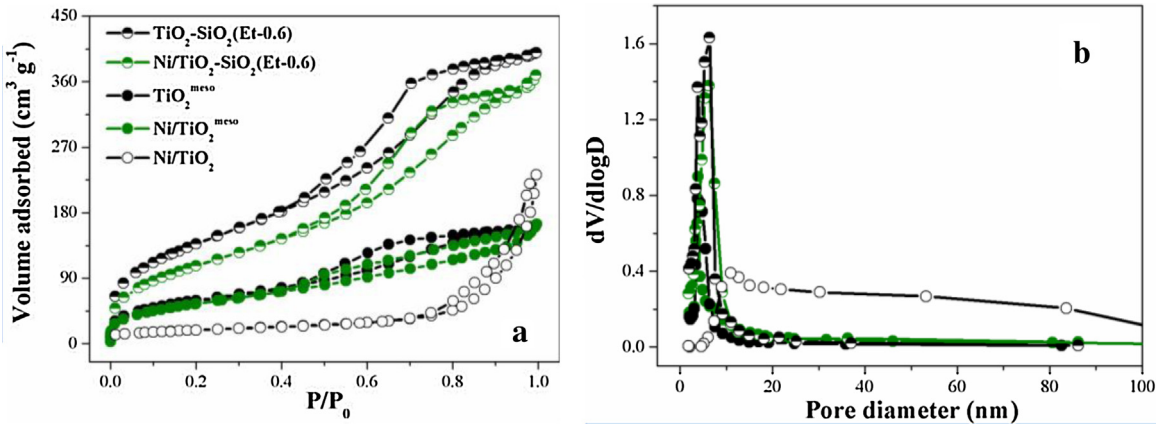

Fig. 3. Nitrogen adsorption–desorption isotherms (a) and pore size distribution profiles (b) of various catalysts and supports.

Table 1
Textural parameters of the supports and catalysts.

Entry	Catalyst	Ni particle size (nm)[a]	Textural property		
			S_{BET} (m^2/g)	D_p (nm)[b]	V_p (cm^3/g)[c]
1	Ni/TiO_2	14	67	11.0	0.25
2	TiO_2	–	120	–	–
3	Ni/TiO_2^{meso}	12	203	3.8	0.23
4	TiO_2^{meso}	–	220	3.8	0.24
5	$Ni/TiO_2–SiO_2$(Et-0.6)	15	404	6.3	0.54
6	$TiO_2–SiO_2$(Et-0.6)	–	511	6.4	0.61

[a] Ni particle size was determined by WXRD measurement.
[b] Pore diameter was estimated from BJH desorption determination.
[c] Pore volume was determined using the adsorption branch of the nitrogen isotherm curve at the P/P_0 = 0.97 single point.

P123 surfactant-assisted co-condensation process was superior to the Ni/TiO_2 prepared using the commercial anatase TiO_2, the BET surface area of Ni/TiO_2^{meso} (203 m^2/g) was triple of Ni/TiO_2 (67 m^2/g). Additionally, as shown in the TEM images (Fig. 4a, c), Ni particles dispersed well on $TiO_2–SiO_2$(Et-0.6) and TiO_2^{meso}, and the average size of Ni particles was approximately 15 and 12 nm, respectively.

3.2. The catalytic performances of $Ni/TiO_2–SiO_2$(Et-x)

At first, the catalytic performance of Ni/TiO_2, Ni/TiO_2^{meso} and $Ni/TiO_2–SiO_2$(Et-x) were compared for the hydrogenation of nitrobenzene in water. As the results displayed in Table 2, the order of catalytic activity for the checked catalysts is $Ni/TiO_2–SiO_2$(Et-x), Ni/TiO_2^{meso} > Ni/TiO_2. With turning the molar ratio of Si/Ti from 0 to 0.6, the conversion of NB changed very less, but the selectivity to aniline increased and simultaneously the selectivity of NSB decreased. The highest selectivity over $Ni/TiO_2–SiO_2$ (Et-0.6) with a Si/Ti of 0.6 reached 97%, which is much higher than that (81.9%) of Ni/TiO_2^{meso} without ethane-bridged organosilica linkage (entries 2–5). It indicates that the suitable amount of ethane-bridged organosilica species could improve the transformation of NSB to AN in H_2O. In addition, the reaction rates in H_2O were much higher than that in ethanol over Ni/TiO_2^{meso} and $Ni/TiO_2–SiO_2$(Et-0.6) (ESI Table S1), indicating H_2O was an effective solvent for the hydrogenation of NB as reported in literature [19–25].

Furthermore, the stability of Ni/TiO_2^{meso}, $Ni/TiO_2–SiO_2$(Et-0.2) and $Ni/TiO_2–SiO_2$(Et-0.6) was examined and compared. During the recycling tests, the catalyst was reused directly without any treatment after separation from the reaction solution, and the end of reaction was judged by the cease of pressure dropping. As the results shown in Table 3, Ni/TiO_2^{meso} deactivated clearly with a decrease in the reaction rate from 98 h^{-1} (the 1st run) to 30 h^{-1} (the 5th run), but it is better than Ni/TiO_2 which deactivated very quickly in the first run with an incomplete conversion as reported in our previous work [27]. While as expected, $Ni/TiO_2–SiO_2$(Et-0.2) and $Ni/TiO_2–SiO_2$(Et-0.6) exhibited improved stability, although the reaction rate presented a little decrease in the first three runs, but it could maintain a constant rate of 103 h^{-1} in the following cycles for $Ni/TiO_2–SiO_2$(Et-0.6).

As we known, the active Ni species is very susceptive and easily to be oxidized with air. Therefore, the Ni-based catalysts are usually pre-reduced and kept in the solvent without exposing to air. Improvement of the air-stability of Ni catalyst is very important and a challenge for the practical applications of Ni-based catalyst. To examine the air-stability, $Ni/TiO_2–SiO_2$(Et-0.6) was collected and stored in a beaker with exposing to air at room temperature for a week, finally the activity and the stability were examined. As shown in Table 3 and Fig. S3c, the initial reaction rate was slow in the 1st run, and to reach complete conversion of NB needed 5 h, but in the 2nd run, the reaction rate increased largely in the first 1 h, and the complete conversion of NB was achieved within 2.8 h. Most importantly, it could keep the similar activity in the following runs. It is deduced that the surface Ni species was oxidized in somewhat as exposed to air, but it could be reduced under the reaction conditions with hydrogen *in-situ*, thus a higher activity was obtained in the following cycles. Therefore, $Ni/TiO_2–SiO_2$(Et-0.6) is an efficient non-noble metal catalyst with high stability to air and water. It is much easier to storage and handle under the atmosphere compared with the Raney nickel and conventional supported Ni catalysts.

4. Discussion

4.1. Hydrophobicity of $Ni/TiO_2–SiO_2$(Et)

When we dispersed the catalysts into the reaction solution of nitrobenzene and water, a biphasic solution was formed due to the low solubility of nitrobenzene in water. Ni/TiO_2^{meso} was dispersed

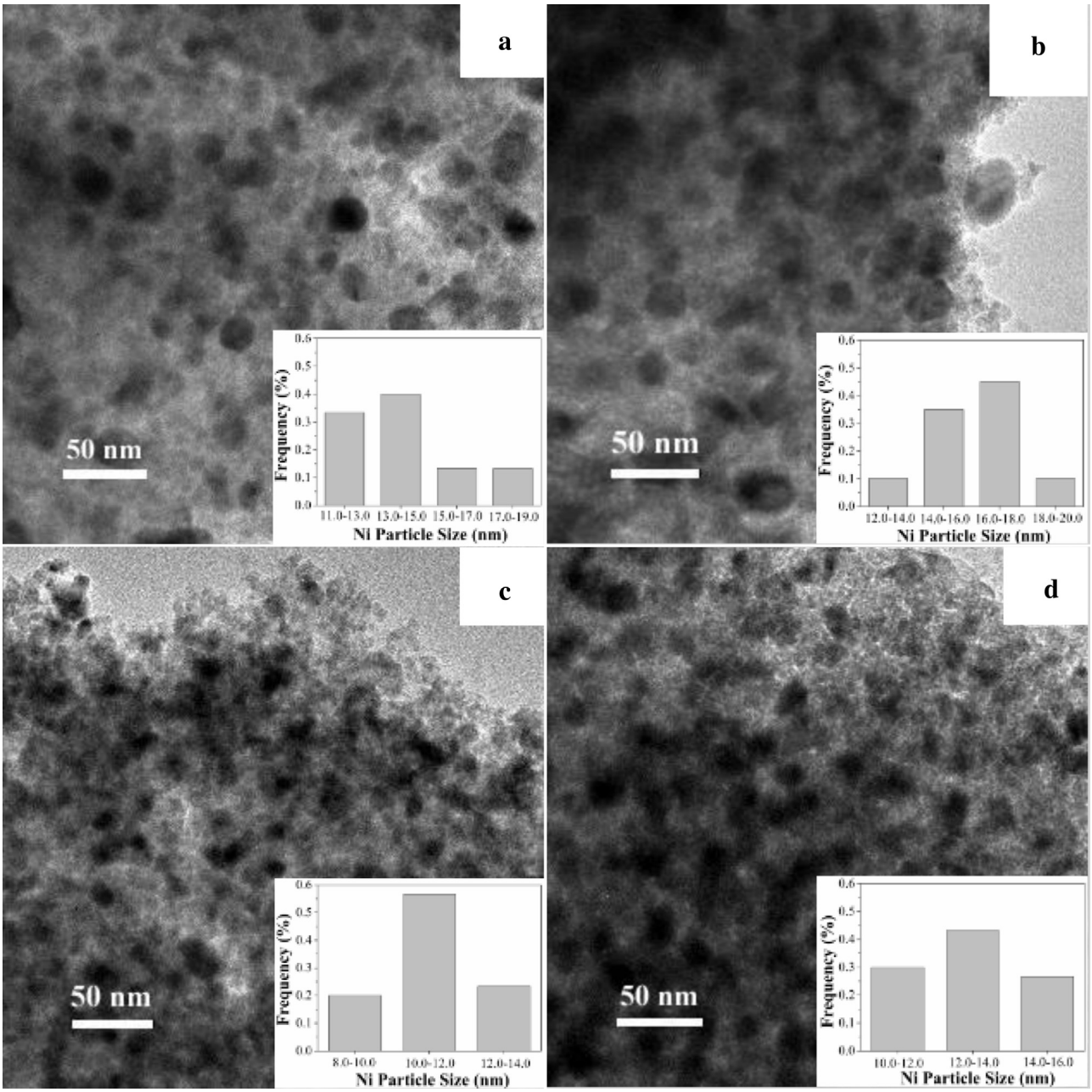

Fig. 4. TEM images of fresh $Ni/TiO_2–SiO_2$(Et-0.6) (a), used $Ni/TiO_2–SiO_2$(Et-0.6) (b), fresh Ni/TiO_2^{meso} (c), and used Ni/TiO_2^{meso} (d), and Ni nanoparticle size distributions was inserted into each TEM image.

Table 2
The catalytic performances of supported Ni catalysts in the hydrogenation of NB.

Entry	Catalyst	Conv. (%)	Sel. (%)[a]			Reaction rate (h^{-1})[b]
			NSB	AN	Others	
1	Ni/TiO_2	49.0	5.6	93.2	1.2	125
2	Ni/TiO_2^{meso}	73.5	17.0	81.9	1.1	188
3	$Ni/TiO_2–SiO_2$(Et-0.2)	72.7	12.5	85.7	1.8	186
4	$Ni/TiO_2–SiO_2$(Et-0.4)	72.8	5.9	93.8	0.3	186
5	$Ni/TiO_2–SiO_2$(Et-0.6)	74.0	2.6	97.0	0.4	189

Reaction conditions: NB: 3 mL, H_2O: 3 mL, H_2: 5 MPa, T: 80 °C, NB/Ni = 256/1 (molar ratio), time: 1 h.

[a] NSB and AN represents nitrosobenzene and aniline, respectively. Others include of *N*-phenylhydroxylamine (PHA), azoxybenzene (AOB), azobenzene (AB) and hydrazobenzene (HAB).

[b] Reaction rate was calculated by the moles of NB converted per mol Ni per hour.

Table 3
Comparison of the reusability of Ni/TiO_2^{meso} and $Ni/TiO_2–SiO_2$(Et-0.6).

Catalyst	Runs	Time (h)	Conv. (%)	Sel. (%)	Reaction rate (h^{-1})[a]
Ni/TiO_2^{meso}	1	2.5	95.3	92.3	98
	2	3.5	99.9	99.9	73
	3	4.5	99.9	99.9	57
	4	7.0	97.0	98.8	35
	5	8.5	99.9	99.8	30
$Ni/TiO_2–SiO_2$(Et-0.2)	1	2.2	99.6	93.2	116
	2	2.5	98.4	95.1	101
	3	3.0	99.9	98.9	85
	4	3.0	99.2	98.0	85
	5	3.0	99.9	98.0	85
$Ni/TiO_2–SiO_2$(Et-0.6)	1	2.0	99.9	99.6	128
	2	2.25	99.6	98.3	113
	3	2.45	98.4	96.1	103
	4	2.45	99.0	97.9	103
	5	2.45	98.9	98.0	103
$Ni/TiO_2–SiO_2$(Et-0.6) (exposed in air for 7 days)	1	5	99.9	95.8	51
	2	2.8	99.9	98.4	91
	3	2	99.9	99.0	128
	4	2.3	99.9	99.8	111
	5	2.8	99.9	99.2	91
	6	2.8	99.9	98.3	91

Reaction conditions: NB: 3 mL, H_2O: 3 mL, H_2: 5 MPa, T: 80 °C, NB/Ni = 256/1 (molar ratio). The reaction was stopped when no more hydrogen consumed.
[a] Reaction rate was calculated by the moles of NB converted per mol Ni per hour.

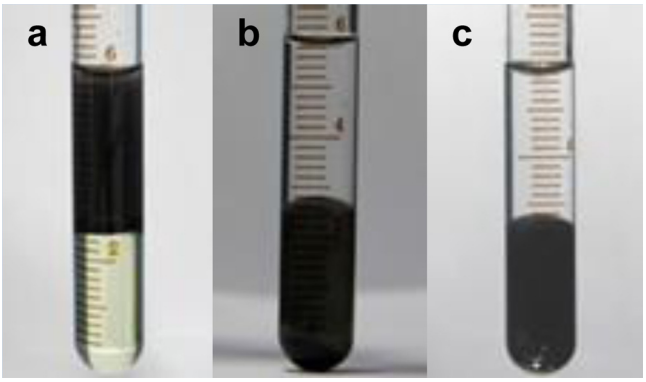

Fig. 5. Distribution of (a) Ni/TiO_2^{meso}, (b) $Ni/TiO_2–SiO_2$(Et-0.2) and (c) $Ni/TiO_2–SiO_2$(Et-0.6) in the mixture of NB and H_2O.

uniformly in the up water layer, while $Ni/TiO_2–SiO_2$(Et-0.2) and $Ni/TiO_2–SiO_2$(Et-0.6) dispersed in the bottom nitrobenzene layer as shown in the Fig. 5. It indicates that $Ni/TiO_2–SiO_2$(Et-x) catalysts were hydrophobic due to incorporated with ethane-bridged organosilica fragments. $Ni/TiO_2–SiO_2$(Et-x) showed similar reaction rate to Ni/TiO_2^{meso} in the presence of water in Table 2 (entries 2–5) as the reaction occurred on the interface of catalysts, the interface area and environment are similar on these two catalysts although they dispersed in different phases. While, the selectivity to AN was much higher over $Ni/TiO_2–SiO_2$(Et-x) than that on Ni/TiO_2^{meso}. The hydrophobic nature of the catalyst is favor to the efficient adsorption and enrichment of organic substrates in the nanopores of hydrophobic materix [33–35]. The NSB may be more prone to adsorb on the hydrophobic $Ni/TiO_2–SiO_2$(Et-x), and then convert to AN quickly.

Furthermore, the catalyst stability was improved significantly after modified with ethane-bridged organosilica (Table 3). $Ni/TiO_2–SiO_2$(Et-0.2) and $Ni/TiO_2–SiO_2$(Et-0.6) presented better stability compared to Ni/TiO_2^{meso}. Ni/TiO_2^{meso} showed a significant deactivation even though it has been improved largely compared to the Ni/TiO_2 catalyst, with which the reaction cannot complete even in the first run, as $Ni(OH)_2$ was formed during the reaction [27]. From WXRD patterns in Fig. 6, the diffraction peaks of metallic Ni

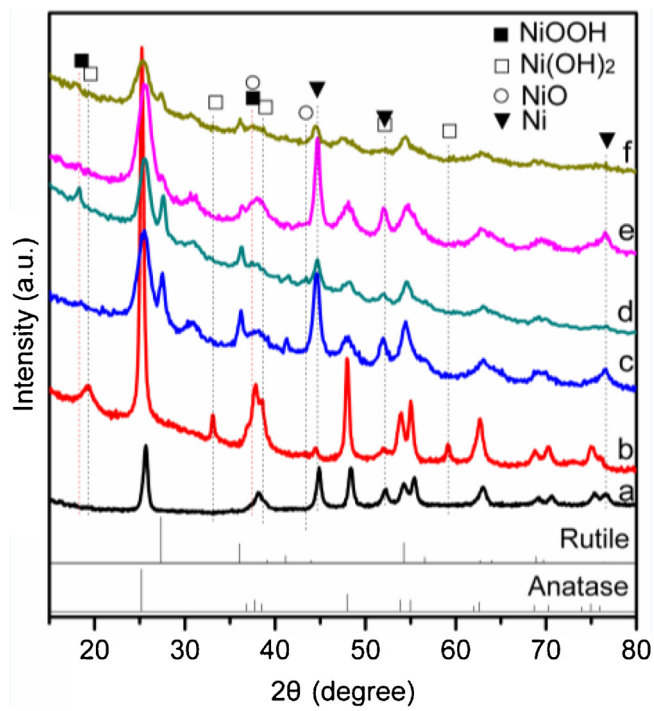

Fig. 6. WXRD patterns of the (a) fresh and (b) used Ni/TiO_2, (c) fresh and (d) used Ni/TiO_2^{meso}, (e) fresh and (f) used $Ni/TiO_2–SiO_2$(Et-0.6). XRD patterns of the fresh and used Ni/TiO_2 reported in Ref. [27].

centred at 2θ of 44.7, 52.1, and 76.6° presented for the fresh Ni/TiO_2, Ni/TiO_2^{meso} and $Ni/TiO_2–SiO_2$(Et-0.6) (Fig. 6a, c, e). For the used Ni/TiO_2, $Ni(OH)_2$ diffraction peaks were detected (Fig. 6b) [27]. For the used Ni/TiO_2^{meso}, the obvious diffraction peaks of NiOOH at 18.3 and 37.3° and the weak peaks of NiO at 37.2 and 43.3° were detected (Fig. 6d). However, these diffraction peaks of $Ni(OH)_2$, NiOOH and NiO were not detected in the used $Ni/TiO_2–SiO_2$(Et-0.6) (Fig. 6f), indicating the hydrophobicity of catalyst could prohibit the contacting of metallic Ni with water to form the Ni oxide/hydroxide species, so the stability of $Ni/TiO_2–SiO_2$(Et-x) was enhanced. The

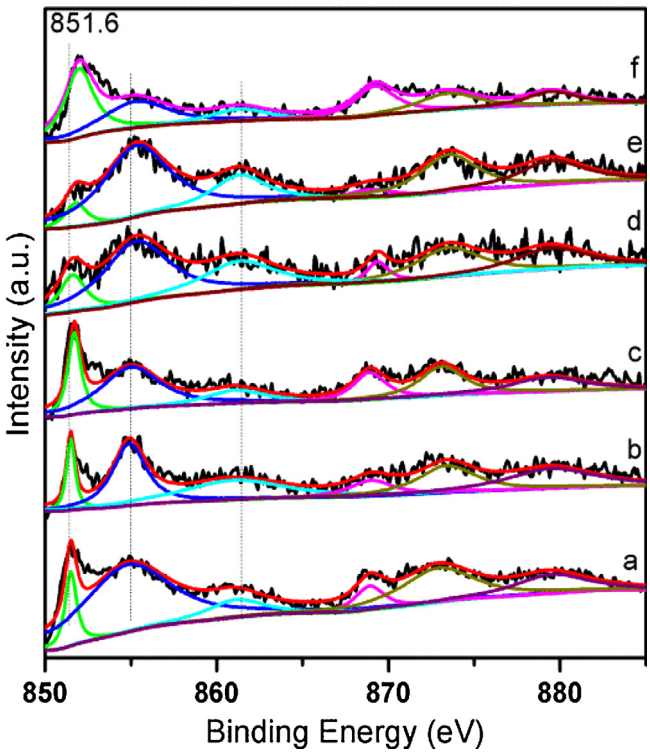

Fig. 7. Ni 2p XPS spectra for the (a) fresh Ni/TiO_2^{meso}, (b) exposed Ni/TiO_2^{meso} in air for 7 days, and (c) sample b was etched for 120 s, and for the (d) fresh Ni/TiO_2–SiO_2(Et-0.6), (e) exposed Ni/TiO_2–SiO_2(Et-0.6) in air for 7 days, and (f) sample e was etched for 120 s.

average sizes of Ni particles was about 15, 12 and 14 nm for the fresh Ni/TiO_2–SiO_2(Et-0.6), Ni/TiO_2^{meso} and Ni/TiO_2, respectively, which are in good agreement with the TEM results in Fig. 4. Ni particle size changed slightly after reaction (Fig. 4b, d), and the leaching of active Ni species could be neglected based on the results of ICP analysis.

4.2. Mesoporous structure of Ni/TiO_2–SiO_2(Et-x)

The enhanced catalytic activity should contribute to the perfect textural properties of catalyst. As revealed by the characterizations, the mesoporous Ni/TiO_2–SiO_2(Et-x) had large BET surface area, high pore volume as well as uniform pore size distribution. Ethane-bridged organosilica fragments were introduced directly and specifically into the TiO_2 network, and participated in the framework of TiO_2/SiO_2(Et) through Ti—O—Si—C—C—Si covalent bonds, which clearly enlarged the pore size of the TiO_2 framework (ESI Table S2). Moreover, the large pore diameter can minimize diffusion problem, whereas large BET surface area may give rise to much more number of the available active sites. Thus, both the larger pore structure and hydrophobicity ensure Ni/TiO_2–SiO_2(Et-0.6) to have higher activity and stability among all the tested catalysts. As illustrated in Table 1, Ni/TiO_2–SiO_2(Et-0.6) exhibited a decrease in pore volume but a similar pore size compared with TiO_2–SiO_2(Et-0.6), suggesting that Ni nanoparticles not only dispersed onto the surface of TiO_2–SiO_2(Et-0.6) but also anchored into the pore channels of TiO_2–SiO_2(Et-0.6), which was further confirmed by XPS analysis. The amount of Ni increased markedly after etching (ESI Table S3) as the exposure of the part of Ni particles located in the pore channels, which should contribute to the air-stability of the catalysts. As the XPS spectra of Ni 2p shown in Fig. 7, Ni/TiO_2^{meso} and Ni/TiO_2–SiO_2(Et-0.6) exposed in air for 7 days (Fig. 7b, e) exhibited the similar results to the fresh ones (Fig. 7a, d), the peak at binding energy of 851.6 eV was assigned to Ni^0, and 855.3 (Ni 2p3/2), 873.5 eV (Ni 2p1/2) were assigned to Ni oxide/hydroxide, and the peaks at binding energies of 861.4 and 879.6 eV should be the satellite peaks of Ni oxide/hydroxide [36–38]. For the samples exposed to the air, the peaks of Ni oxide/hydroxide was a little larger compared to the fresh ones as Ni^0 species were somewhat oxidized by air. However, after etching for 120 s (Fig. 7c, f), the peak of Ni^0 at 851.6 eV became intense and the peaks Ni oxide/hydroxide at 855.3 and 873.5 eV decreased largely. That is to say, most of the Ni^0 particles might be anchored into the mesoporous channel and matrix, which could effectively reduce the oxidation degree of Ni, and so Ni/TiO_2–SiO_2(Et-0.6) is relative air-stable and could be stored in air and recycled successfully. In addition, the mesoporous channels may favor the hydrogenation of NB, and the activity of Ni/TiO_2^{meso} was much higher than that of Ni/TiO_2 (entries 1,2 in Table 2). The mesoporous channels could somewhat protect the Ni particles from the corrosion of water, Ni/TiO_2^{meso} could be reused for five times (Table 3), but Ni/TiO_2 deactivated completely in the first run [27].

In summary, the enhanced hydrophobic property, high dispersion of the Ni particles into the mesoporous TiO_2–SiO_2(Et) as well as their stronger interactions are benefit for the outstanding activity and unexpected stability to air and water.

5. Conclusions

A novel mesostructured Ni/TiO_2–SiO_2(Et) catalyst with highly dispersed Ni nanoparticles was successfully prepared. The Ni/TiO_2–SiO_2(Et) catalysts exhibited high catalytic activity and stability toward the hydrogenation of nitrobenzene in water. These unique catalytic performances of the Ni/TiO_2–SiO_2(Et) catalyst were mainly due to the incorporation of the hydrophobic group (ethane-bridged organosilica moieties) into TiO_2 network, creating a combination of increased hydrophobicity with well-defined mesoporosity, which leads to a remarkable enhancement in the catalytic activity and stability in water. The current studies confirmed that the as-prepared Ni/TiO_2–SiO_2(Et) is an excellent water-tolerable and air-stable heterogeneous catalyst. It is expected to have a wide application in the selective hydrogenation reactions in water.

Acknowledgements

This work is supported by the Natural Science Fund Council of China (NO. 21273222 and 21202159), and China postdoctoral science foundation (NO. 2013M531000).

Appendix A. Supplementary data

Supplementary data associated with this article can be found, in the online version, at http://dx.doi.org/10.1016/j.molcata.2015.10.023.

References

[1] Y.F. Zheng, K. Ma, H.L. Wang, X. Sun, J. Jiang, C.F. Wang, R. Li, J.T. Ma, Catal. Lett. 124 (2008) 268–276.
[2] X.C. Meng, H.Y. Cheng, Y. Akiyama, Y.F. Hao, W.B. Qiao, Y.C. Yu, F.Y. Zhao, S. Fujita, M. Arai, J. Catal. 264 (2009) 1–10.
[3] Y.E. Wu, S.F. Cai, D.S. Wang, W. He, Y.D. Li, J. Am. Chem. Soc. 134 (2012) 8975–8981.
[4] S.A. Regenhardt, C.I. Meyer, T.F. Garetto, A.J. Marchi, Appl. Catal. A: Gen. 449 (2012) 81–87.
[5] Y. Wang, X.Y. Chen, B. Yue, H.Y. He, Top. Catal. 55 (2012) 1022–1031.
[6] B. Legras, V.V. Ordomsky, C. Dujardin, M. Virginie, A.Y. Khodakov, ACS Catal. 4 (2014) 2785–2791.
[7] C.M. Li, Y.D. Chen, S.T. Zhang, J.Y. Zhou, F. Wang, S. He, M. Wei, D.G. Evans, X. Duan, ChemCatChem 6 (2014) 824–831.
[8] J.X. Chen, T. Guo, K.L. Li, L.M. Sun, Catal. Sci. Technol. 5 (2015) 2670–2680.

[9] P.S. Rathore, R. Patidar, T. Shripathi, S. Thakore, Catal. Sci. Technol. 5 (2015) 286–295.
[10] D.H. Kim, H.O. Seo, M.G. Jeong, Y.D. Kim, Catal. Lett. 144 (2014) 56–61.
[11] Z. Yang, Y.B. Huang, Q.X. Guo, Y. Fu, Chem. Commun. 49 (2013) 5328–5330.
[12] Z.M. Rong, Z.H. Sun, L. Wang, J.K. Lv, Y. Wang, Y. Wang, Catal. Lett. 144 (2014) 1766–1771.
[13] S.J. Tauster, Acc. Chem. Res. 20 (1987) 389–394.
[14] A. Corma, P. Serna, P. Concepcion, J.J. Calvino, J. Am. Chem. Soc. 130 (2008) 8748–8753.
[15] B. Coq, A. Tijani, R. Dutartre, F. Figueras, J. Mol. Catal. 79 (1993) 253–264.
[16] X.X. Han, R.X. Zhou, G.H. Lai, X.M. Zheng, Catal. Today 93–95 (2004) 433–437.
[17] J. Xiong, J.X. Chen, J.Y. Zhang, Catal. Commun. 8 (2007) 345–350.
[18] Y.Z. Xiang, X.N. Li, C.S. Lu, L. Ma, Q.F. Zhang, Appl. Catal. A: Gen. 375 (2010) 289–294.
[19] J.B. Ning, J. Xu, J. Liu, H. Miao, H. Ma, C. Chen, X.Q. Li, L.P. Zhou, W.Q. Yu, Catal. Commun. 8 (2007) 1763–1766.
[20] M. Pietrowski, M. Zielinski, M. Wojciechowska, Catal. Lett. 128 (2009) 31–35.
[21] G.Y. Fan, L. Zhang, H.Y. Fu, M.L. Yuan, R.X. Li, H. Chen, X.J. Li, Catal. Commun. 11 (2010) 451–455.
[22] K. Taya, Sci. Papers I.P.C.R. 56 (1962) 285–289.
[23] J.H. Lyu, X.B. He, C.S. Lu, L. Ma, Q.F. Zhang, F. Feng, X.N. Li, J.G. Wang, Chin. Chem. Lett. 25 (2014) 205–208.
[24] Y.F. Hao, R.X. Liu, X.C. Meng, H.Y. Cheng, F.Y. Zhao, J. Mol. Catal. A: Chem. 335 (2011) 183–188.
[25] X.C. Meng, H.Y. Cheng, S. Fujita, Y.C. Yu, F.Y. Zhao, M. Arai, Green Chem. 13 (2011) 570–572.
[26] M. Jorge, M.N.D.S. Cordeiro, J. Phys.Chem. C 111 (2007) 17612–17626.
[27] W.W. Lin, H.Y. Cheng, J. Ming, Y.C. Yu, F.Y. Zhao, J. Catal. 291 (2012) 149–154.
[28] W. Li, F.Y. Ma, F. Su, L. Ma, S.Q. Zhang, Y.H. Guo, ChemSusChem 4 (2011) 744–756.
[29] W. Li, F.Y. Ma, F. Su, L. Ma, S.Q. Zhang, Y.H. Guo, ChemCatChem 4 (2012) 1798–1807.
[30] L. Zhao, G.S. Zhu, D.L. Zhang, Y. Di, Y. Chen, O. Terasaki, S.L. Qiu, J. Phys. Chem. B 109 (2005) 764–768.
[31] J. Ming, C.Y. Wu, H.Y. Cheng, Y.C. Yu, F.Y. Zhao, J. Supercrit. Fluids 57 (2011) 137–142.
[32] J. Ming, H.Y. Cheng, Y.C. Yu, Y.Q. Wu, F.Y. Zhao, J. Mater. Chem. 21 (2011) 6654–6659.
[33] F.J. Liu, L. Wang, Q. Sun, L.F. Zhu, X.J. Meng, F.S. Xiao, J. Am. Chem. Soc. 134 (2012) 16948–16950.
[34] L. Wang, J. Zhang, J. Sun, L.F. Zhu, H.Y. Zhang, F.J. Liu, D.F. Zheng, X.J. Meng, X.D. Shi, F.S. Xiao, ChemCatChem 5 (2013) 1606–1613.
[35] L. Wang, F.S. Xiao, ChemCatChem 6 (2014) 3048–3052.
[36] Z.Y. Hou, O. Yokota, T. Tanaka, T. Yashima, Appl. Catal. A: Gen. 253 (2003) 381–387.
[37] N. Mahata, A.F. Cunha, J.J.M. Orfao, J.L. Figueiredo, Appl. Catal. A: Gen. 351 (2008) 204–209.
[38] N. Mahata, A.F. Cunha, J.J.M. Orfao, J.L. Figueiredo, ChemCatChem 2 (2010) 330–335.